Experimental investigation of the stronger uncertainty relations for all incompatible observables

Kunkun Wang,[1] Xiang Zhan,[1] Zhihao Bian,[1] Jian Li,[1] Yongsheng Zhang,[2,3,*] and Peng Xue[1,†]

[1]*Department of Physics, Southeast University, Nanjing 211189, China*

[2]*Key Laboratory of Quantum Information, University of Science and Technology of China, Chinese Academy of Sciences, Hefei 230026, China*

[3]*Synergetic Innovation Center of Quantum Information and Quantum Physics, University of Science and Technology of China, Hefei 230026, China*

(Received 23 November 2015; revised manuscript received 16 April 2016; published 11 May 2016)

The Heisenberg-Robertson uncertainty relation quantitatively expresses the impossibility of jointly sharp preparation of incompatible observables. However, it does not capture the concept of incompatible observables because it can be trivial even for two incompatible observables. We experimentally demonstrate that the new stronger uncertainty relations proposed by Maccone and Pati [Phys. Rev. Lett. **113**, 260401 (2014)] relating to the sum of variances are valid in a state-dependent manner and that the lower bound is guaranteed to be nontrivial when two observables are incompatible on the state of the system being measured. The behavior we find agrees with the predictions of quantum theory and obeys the new uncertainty relations even for the special states which trivialize the Heisenberg-Robertson relation. We realize a direct measurement model and perform an experimental investigation of the strengthened relations.

DOI: 10.1103/PhysRevA.93.052108

I. INTRODUCTION

The famous uncertainty relation introduced by Werner Heisenberg is a basic feature of quantum theory enshrined in all textbooks [1,2]. The uncertainty principle dramatically illustrates the difference between classical and quantum mechanics. The principle bounds the uncertainties about the outcomes of two incompatible measurements, such as position and momentum on a particle. The more precisely the position of a particle is determined, the less precisely its momentum can be known, and vice versa. This lack of knowledge, so-called uncertainty, was quantified by Heisenberg using the standard deviation. If the measurement on a given particle is chosen from a set of two possible observables A and B, the resulting bound on the uncertainty can be expressed in terms of the commutator,

$$\Delta A^2 \Delta B^2 \geqslant \left|\tfrac{1}{2}\langle [A,B]\rangle\right|^2, \tag{1}$$

which is the so-called Heisenberg-Robertson uncertainty relation [3].

Uncertainty relations are useful for a wide range of applications in quantum technologies including quantum cryptography, quantum entanglement, quantum computation, and general physics. In detail, they are useful for formulating quantum mechanics [4,5] (e.g., to justify the complex structure of the Hilbert space or as a fundamental building block for quantum mechanics and quantum gravity), for studying measurement-induced disturbance [6–9], for entanglement detection [10–12], for security analysis of quantum cryptography [13,14], and so on. Uncertainty relations were tested experimentally with neutronic [15–17] and photonic qubits [18–23].

However, the Heisenberg-Robertson relation (1) does not fully capture the notion of incompatible observables since it is expressed in terms of the *product* of the variances of measurements of the observables. It means the product is zero when either of the two variances is zero even if the other variance is nonzero. This is the flaw in the Heisenberg-Robertson relation.

To overcome this limitation, Maccone and Pati [24] have proposed two new uncertainty relations that employ the *sum* of the variances of measurements of general observables. Since the variance is a positive quantity, the sum will always be nonzero unless both variances are zero and this case only happens if the observables are "compatible," meaning they have a definite value.

We report an experimental test of the new uncertainty relations for a single-photon measurement and demonstrate that they are valid for states of a spin-1 particle [25]. Compared to the previous experiments which have come close to the original uncertainty limit [26–30] but did not overcome the inherent flaw, our experimental results fully capture the notion of incompatible observables in contrast to the Heisenberg-Robertson inequality, thus making the uncertainty relations much stronger. The results also explain so-called complementarity—an extreme form of uncertainty (here variance is used as a measure of uncertainty); i.e., one of the two properties of a system is perfectly known, and the other is completely uncertain, which is a situation that the Heisenberg-Robertson inequality fails to explain. Furthermore, in our experiment, every term can be obtained directly by the outcomes of the projective measurements. Our test realizes a direct measurement model which releases the requirement of quantum state tomography [18,19].

II. THEORETICAL FRAMEWORK

Consider two observables A and B which are incompatible on the state $|\psi\rangle$. The new stronger uncertainty relations proposed by Maccone and Pati relating to the sum of variances are theoretically proven to be universally valid [24]. The first inequality [24] is

$$\Delta A^2 + \Delta B^2 \geqslant \pm i\langle [A,B]\rangle + |\langle \psi|A \pm iB|\psi^{\perp}\rangle|^2, \tag{2}$$

*yshzhang@ustc.edu.cn
†gnep.eux@gmail.com

where the sign should be chosen so that $\pm i\langle[A,B]\rangle$ (a real quantity) is positive. The inequality is valid for an arbitrary state $|\psi^\perp\rangle$ orthogonal to $|\psi\rangle$. If the state $|\psi\rangle$ is not a joint eigenstate of A and B, the lower bound of the inequality is nontrivial (nonzero) for almost any choice of $|\psi^\perp\rangle$. The uncertainty inequality in (2) is tight; i.e., it becomes an equality by maximizing over $|\psi^\perp\rangle$. For example, if $|\psi\rangle$ is one of the eigenstates of the observable A, the optimal choice of $|\psi^\perp\rangle$ is $|\psi^\perp\rangle_B = (B - \langle B\rangle)|\psi\rangle/\Delta B$, or $|\psi^\perp\rangle_A = (A - \langle A\rangle)|\psi\rangle/\Delta A$ for the case that $|\psi\rangle$ is one of the eigenstates of the observable B. If $|\psi\rangle$ is not an eigenstate of either, the optimal choice is $|\psi^\perp\rangle \propto (A \pm iB - \langle A \pm iB\rangle)|\psi\rangle$.

The second inequality with nontrivial bound [24] is

$$\Delta A^2 + \Delta B^2 \geqslant \tfrac{1}{2}|_{A+B}\langle\psi^\perp|A+B|\psi\rangle|^2, \tag{3}$$

where $|\psi^\perp\rangle_{A+B} \propto (A + B - \langle A + B\rangle)|\psi\rangle$ is orthogonal to $|\psi\rangle$. The lower bound of Eq. (3) is nonzero unless $|\psi\rangle$ is an eigenstate of $A + B$. The inequality (3) becomes an equality if the state $|\psi\rangle$ is an eigenstate of $A - B$.

We show an example by choosing two components of the angular momentum for a spin-1 particle as two incompatible observables

$$A = J_x = \begin{pmatrix} 0 & 1 & 0 \\ 1 & 0 & 1 \\ 0 & 1 & 0 \end{pmatrix}$$

and

$$B = J_y = \begin{pmatrix} 0 & i & 0 \\ -i & 0 & i \\ 0 & -i & 0 \end{pmatrix},$$

and a family of states being measured [24],

$$|\psi_\phi\rangle = \sin\phi|+\rangle + \cos\phi|-\rangle = (\sin\phi, 0, \cos\phi)^{\mathrm{T}}, \tag{4}$$

where $|\pm\rangle$ are the eigenstates of

$$J_z = \begin{pmatrix} 1 & 0 & 0 \\ 0 & 0 & 0 \\ 0 & 0 & -1 \end{pmatrix}$$

corresponding to the eigenvalues ± 1, and $\phi \in [0,\pi]$ is the coefficient. None of $|\psi_\phi\rangle$ is a joint eigenstate of J_x and J_y, nor are they an eigenstate of $J_x + J_y$. The uncertainty relations in inequalities (2) and (3) are valid for the states. However, for the special cases with $\phi = \pi/4$ and $\phi = 3\pi/4$, the Heisenberg-Robertson relation can be trivial because one of the measurement variances is zero.

Now we focus on the feasibility of implementation of the measurements. The variances $\Delta J_{x(y)} = \langle J^2_{x(y)}\rangle - \langle J_{x(y)}\rangle^2$ can be calculated by the measured expectation values of $J_{x(y)}$ and $J^2_{x(y)}$. The first term on the right-hand side (RHS) of inequality (2) can be calculated by the measured expectation value of $J_z = i[J_x, J_y]/2$. The second term can be rewritten as $|\langle\psi_\phi|J_x \pm iJ_y|\psi^\perp_\phi\rangle|^2 = \langle\psi_\phi|C_\pm|\psi_\phi\rangle$, where

$$C_\pm := (J_x \pm iJ_y)|\psi^\perp_\phi\rangle\langle\psi^\perp_\phi|(J_x \mp iJ_y) \tag{5}$$

are Hermitian operators. The second term on the RHS of inequality (2) can be calculated by the expectation values of the operators $C_\pm$. Inequality (2) can be rewritten as $\Delta J_x^2 + \Delta J_y^2 \geqslant |\langle J_z\rangle| + \langle C_\pm\rangle$.

Similarly, inequality (3) can be rewritten as $\Delta J_x^2 + \Delta J_y^2 \geqslant \langle D\rangle$, where the observable of the measurement is

$$D := \tfrac{1}{2}(J_x + J_y)|\psi^\perp_\phi\rangle_{J_x+J_y}\langle\psi^\perp_\phi|(J_x + J_y). \tag{6}$$

The observables $C_\pm$ and D are dependent on the choices of the states $|\psi^\perp_\phi\rangle$ and $|\psi^\perp_\phi\rangle_{J_x+J_y}$, respectively. Although the second inequality is tight also, for the family of states in Eq. (4) which are not the eigenstates of $J_x \pm J_y$, the inequality will not become an equality for any choice of $|\psi^\perp_\phi\rangle_{J_x+J_y}$.

III. EXPERIMENTAL IMPLEMENTATION

We report the experimental test of the new uncertainty relations for a single-photon measurement. The experimental setup shown in Fig. 1 involves preparing the specific state (state preparation stage) and projective measurement on the system of interest (measurement stage). In the preparation stage, polarization-degenerate photon pairs at a wavelength of 801.6 nm are produced in a type I spontaneous parametric down-conversion (SPDC) source using a 0.5-mm-thick β-barium borate (BBO) nonlinear crystal, pumped by a cw diode laser with 90 mW of power [31–34]. The pump is filtered out with the help of an interference filter which restricts the photon bandwidth to 3 nm. With the detection of a trigger photon, the signal photon is heralded in the measurement setup. Experimentally this trigger-signal photon pair is registered by a coincidence count at two single-photon avalanche photodiodes (APDs) with 7-ns time window. Total coincidence counts are about 1×10^4 over a collection time of 6 s.

A qutrit is represented by three modes of the heralded single photons shown in Fig. 1(a), and the basis states $|0\rangle$, $|1\rangle$, and $|2\rangle$ are encoded by the horizontal polarization of the photon in the upper mode, the horizontal polarization of the

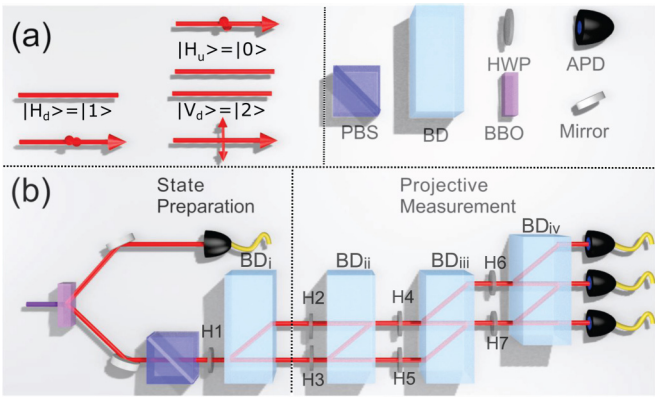

FIG. 1. (a) Representation of a qutrit. Here H and V denote the horizontal and vertical polarizations of the single photons, respectively. The subscripts u and d represent the upper and lower spatial modes of the single photons, respectively. (b) Experimental setup. The herald single photons are created via type I spontaneous parametric down-conversion in a BBO crystal and are injected into the optical network. The polarizing beam splitter (PBS), half-wave plate (HWP, H1), and beam displacer (BD_i) are used to generate a qutrit state $|\psi_\phi\rangle$. The HWPs (H2–H7) and three BDs are used to realize the projective measurements of observables $J_{x(y)}$, $J^2_{x(y)}$, and $C_\pm$. To realize that of D, H4 and H5 are replaced by the QWPs (Q4 and Q5) at 45°.

photon in the lower mode, and the vertical polarization in the lower mode, respectively. The heralded single photons pass through a polarizing beam splitter (PBS) and a half-wave plate (HWP, H1) with a certain setting angle and then are split by a birefringent calcite beam displacer (BD) into two parallel spatial modes—upper and lower modes [35,36]. The optical axis of the BD is cut so that vertically polarized light is directly transmitted and horizontal light undergoes a 3-mm lateral displacement into a neighboring mode. Thus the photons are prepared in the state $|\psi_\phi\rangle$ in Eq. (4). We choose $\phi = j\pi/12$ ($j = 1,\ldots,12$), i.e., a total of 12 states, for testing the uncertainty relation proposed in Ref. [24]. The setting angle $\theta_1(\phi)$ of H1 used for generating the state $|\psi_\phi\rangle$ satisfies $\theta_1(\phi) = \pi/4 - \phi/2$.

For the left-hand side (LHS) of inequalities (2) and (3), the upper bound is $\Delta J_x^2 + \Delta J_y^2 = 1$, which is constant for all 12 states being measured. For half of the states with $\phi = \pi/12,\pi/6,\pi/4,5\pi/6,11\pi/12,\pi$, because of $i\langle[J_x,J_y]\rangle \leqslant 0$, the RHS of inequality (2) can be rewritten as $2|\langle J_z\rangle| + \langle C_-\rangle$, whereas for the remaining six states being measured, it is $2|\langle J_z\rangle| + \langle C_+\rangle$.

In the measurement stage, cascaded interferometers which consist of BDs and wave plates (WPs) are used to implement an operation $U = \sum_i |i\rangle\langle m_i|$, where $|m_i\rangle$ ($i = 0,1,2$) is the eigenstate of the observable $M = \sum_i m_i|m_i\rangle\langle m_i|$ according to the eigenvalue m_i. The BD_{iv} is used to map the basis states of the qutrit to three spatial modes and to accomplish the projective measurement $\{|m_0\rangle\langle m_0|,|m_1\rangle\langle m_1|,|m_2\rangle\langle m_2|\}$ of the observable M on a qutrit state $|\psi_\phi\rangle$ along with APDs. The outcomes give the measured probability $p_{m_i} = |\langle\psi_\phi|m_i\rangle|^2$, which equals the probability $p_i = \mathrm{Tr}(|\psi_\phi\rangle\langle\psi_\phi|U^\dagger|i\rangle\langle i|U)$ of the photons being measured in the state $|i\rangle$. The expected value of the observable M can be calculated by the measured probabilities and the eigenvalues as $\langle M\rangle = \sum_i m_i p_{m_i}$. Similarly one can calculate the variance ΔM of M with the outcomes of the projective measurements on the state $|\psi_\phi\rangle$.

To test the inequalities, we need to measure the observables $J_{x(y)}$, $J_{x(y)}^2$, J_z, and $C_\pm$ in Eq. (5) and D in Eq. (6) (see Appendix B). The unitary operation which performs a projective measurement is SU(3), which can be realized in three substeps. Each of the substeps applies a rotation on two of the basis states $\{|0\rangle,|1\rangle,|2\rangle\}$ and keeps the remaining one unchanged. Each of the substeps can be realized by two HWPs and a BD. One of the HWPs is used to rotate the qutrit, the other is used to compensate for the optical delay, and the BD is used to split the photons with different polarizations into different modes. The setting angles of H3, H4, and H7 (or H6) can be calculated by the parameters of the projective measurement, the setting angles of H2 and H5 are chosen to be 45°, and that of H6 is 0° (or that of H7 is −45°) to compensate for the optical delay. The photons are detected by APDs, in coincidence with the trigger photons. The probabilities p_i ($i = 0,1,2$) are obtained by normalizing photon counts in the ith spatial mode to total photon counts.

To test the first inequality (2), for the 12 states $|\psi_\phi\rangle$ we choose, the optimization of $|\psi_\phi^\perp\rangle$ (namely, the choice that maximizes the lower bound and saturates the inequality) is independent of ϕ and takes the form

$$|\psi_\phi^\perp\rangle_{\mathrm{opt}} = (0,1,0)^{\mathrm{T}}. \tag{7}$$

Then for each ϕ, we randomly choose three states

$$\begin{aligned}
|\psi_\phi^\perp\rangle_1 &= \frac{\sqrt{3}}{2}\left(\cos\phi, \frac{\sqrt{3}}{3}, -\sin\phi\right)^{\mathrm{T}},\\
|\psi_\phi^\perp\rangle_2 &= \frac{\sqrt{2}}{2}(\cos\phi, 1, -\sin\phi)^{\mathrm{T}},\\
|\psi_\phi^\perp\rangle_3 &= \frac{1}{2}(\cos\phi, \sqrt{3}, -\sin\phi)^{\mathrm{T}},
\end{aligned} \tag{8}$$

which are orthogonal to $|\psi_\phi\rangle$ to test inequality (2). For the optimal choice of the orthogonal state $|\psi_\phi^\perp\rangle_{\mathrm{opt}}$, as well as the three others $|\psi_\phi^\perp\rangle_{1,2,3}$, the projective measurement of observable $C_\pm$ can be realized by tuning the setting angles of the HWPs (H2–H7) (see Appendix A).

Similarly, to test the second inequality (3), the measurement of the observable D in Eq. (6) can be implemented by the setup in Fig. 1(b) by replacing the HWPs (H4 and H5) by the quarter-wave plates (QWPs, Q4 and Q5, respectively) and setting angles 45° for all 12 states $|\psi_\phi\rangle$.

In Fig. 2, we show the direct demonstration of the two new uncertainty relations in inequalities (2) and (3). The LHS of inequalities (2) and (3), i.e., the sum of the uncertainties $\Delta J_x^2 + \Delta J_y^2$, is constant for the family of states in Eq. (4) as $\Delta J_x^2 + \Delta J_y^2 = 1$. The experimental results of the LHS of the inequalities are calculated from the measured data of observables $J_{x(y)}$ and $J_{x(y)}^2$ and fit the theoretical predictions well. The experimental results of the RHS of inequality (2) with the optimal choice of the state $|\psi_\phi^\perp\rangle_{\mathrm{opt}}$ and the states $|\psi_\phi^\perp\rangle_{1,2,3}$ which are chosen randomly are shown with different symbols. It is clear that the bound (2) is always

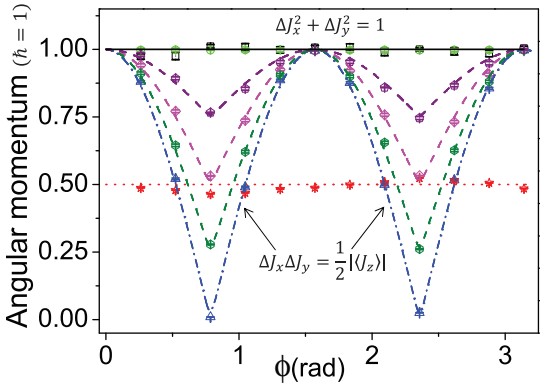

FIG. 2. Experimental results. The solid black line corresponds to the LHS of inequalities (2) and (3), i.e., $\Delta J_x^2 + \Delta J_y^2 = 1$. The black squares represent the sum of the measured uncertainties of ΔJ_x^2 and ΔJ_y^2 with the 12 states $|\psi_\phi\rangle$. The green circles, olive hexagons, magenta diamonds, and purple pentagons represent the experimental results of the RHS of inequality (2) with the optimal state $|\psi_\phi^\perp\rangle_{\mathrm{opt}}$ and three randomly chosen states $|\psi_\phi^\perp\rangle_{1,2,3}$ for each of the 12 values of ϕ. The red dotted line corresponds to the bound of inequality (3) and red stars represent the measured $\langle D\rangle$ for the 12 states $|\psi_\phi^\perp\rangle_{J_x+J_y}$. The blue dot-dashed curves and triangles represent the theoretical predictions and experimental results of the product of the uncertainties and the expectation value of the commutator (Heisenberg-Robertson relation). Error bars indicate the statistical uncertainty.

satisfied and outperforms the Heisenberg-Robertson relation for arbitrary states $|\psi_\phi^\perp\rangle$ orthogonal to $|\psi_\phi\rangle$. All data of the RHS are above the lower curves, which are the product of the uncertainties and the expectation value of the commutator. Thus the new uncertainty relation in inequality (2) is more strengthened compared to the Heisenberg-Robertson relation. For the optimal choice $|\psi_\phi^\perp\rangle_{\rm opt}$, which is independent of ϕ, the experimental results fit the upper bound well. Thus the inequality becomes an equality, which shows the new uncertainty inequality (2) is tight.

For inequality (3), due to the orthogonal state

$$|\psi_\phi^\perp\rangle_{J_x+J_y} = (0,1,0)^{\rm T}, \tag{9}$$

which is independent of ϕ, the theoretical prediction of the RHS is constant as $\langle D\rangle = 0.5$, which fits our data well and satisfies the uncertainty inequality.

Our experimental results show that for the state $|\psi_\phi\rangle$ that is an eigenstate of one of the two observables (in our case, $\phi = \pi/4$ and $\phi = 3\pi/4$) which trivializes the Heisenberg-Robertson relation, the lower bound of the new uncertainty inequalities is always nontrivial unless $|\psi_\phi\rangle$ is a joint eigenstate of the two observables.

As in previous experiments [18,19], both sides of inequalities (2) and (3) can be calculated from the density matrices of $|\psi_\phi\rangle$, which are characterized by quantum state tomography. In our experiment, every term of the inequalities can be obtained directly by the outcomes of the projective measurements, and the experimental results are in good agreement with theoretical predictions. Our test realizes a direct measurement model which much simplifies the experimental realization and releases the requirement of quantum state tomography. It is much more "user friendly" compared to those that require reconstruction of the state being measured by carrying out a set of measurements through tomographic means and calculating the expected values of the measurement of observables.

Furthermore, our technique can be used to realize arbitrary SU(3) unitary operation and arbitrary projective measurements of a qutrit. An arbitrary SU(3) unitary operation on a qutrit can be decomposed into three matrices which can be realized by a transformation on two modes of the qutrit, keeping the third mode unaffected [37,38]. Conveniently, two-mode transformations can then be implemented using WPs acting on the two polarization modes propagating in the same spatial mode. Thus we are able to apply transformations to any pair of modes.

IV. CONCLUSION

We have demonstrated a method for experimentally testing the new uncertainty relations. This has allowed us to test the two uncertainty inequalities. Our experimental results clearly illustrate the new uncertainty relations between two components of the angular momentum. Our demonstration is evidence for the validity of the new relations proposed to be universally valid. Our work conclusively shows that the new uncertainty relations are stronger and general compared to the Heisenberg-Robertson uncertainty relation. The experimental results confirm that, even for the special states which trivialize the Heisenberg-Robertson relation, the uncertainties of the two observables obey the new relations and shed light on the fundamental limitations of quantum measurement. A correct understanding and experimental confirmation of a fundamental limitation of measurements will not only foster insight into foundational problems but also advance the precision measurement technology in quantum information processing, for instance on the debate over the standard quantum limit for monitoring free-mass position [39–41].

ACKNOWLEDGMENTS

We acknowledge support by NSFC (Grants No. 11474049 and No. 61275122). We thank L. Maccone and A. K. Pati for their helpful discussion.

APPENDIX A: VERIFY THE NEW UNCERTAINTY RELATIONS WITH A THREE-LEVEL SYSTEM

The photonic states $|\psi_\phi\rangle$ can be generated in a type I SPDC process. For different ϕ, one can vary the setting angle of the HWP (H1). The angles of the HWPs for state preparation are listed in Table I. The density matrix of the initial state $|\psi_\phi\rangle$ is characterized by the quantum state tomography process with nine measurement settings and the average fidelity for the 12 states is more than 0.988.

In the measurement stage, cascaded interferometers which consist of BDs and WPs are used to implement projective measurements of the observables $J_{x(y)}$, J_z, $J_{x(y)}^2$, $C_\pm$, and D. The angles of the HWPs (H2–H7) for state preparation are listed in Table II. For some observables, we replace the HWPs (H4 and H5) by QWPs (Q4 and Q5) with setting angles 45°. The polarization analysis measurement setup containing QWPs, HWPs, and BDs can be used to perform measurements of the corresponding observable on photons.

The technique of direct state transformations with optical elements we use here can realize arbitrary SU(3) unitary operation and arbitrary projective measurements of a qutrit. An arbitrary SU(3) unitary operation on a qutrit can be decomposed into three matrices which can be realized by a transformation on two modes of the qutrit, keeping the third mode unaffected. Conveniently, two-mode transformations can then be implemented using WPs acting on the two polarization modes propagating in the same spatial mode. Thus we are able to apply transformations to any pair of modes.

Now we show an example of how to realize the measurement of observable J_x via WPs and BDs and the state

TABLE I. The setting angles of the HWP (H1) for the state preparation stage.

ϕ (rad)	$\frac{\pi}{12}$	$\frac{\pi}{6}$	$\frac{\pi}{4}$	$\frac{\pi}{3}$	$\frac{5\pi}{12}$	$\frac{\pi}{2}$	$\frac{7\pi}{12}$	$\frac{2\pi}{3}$	$\frac{3\pi}{4}$	$\frac{5\pi}{6}$	$\frac{11\pi}{12}$	π
H1	37.50°	30.00°	22.50°	15.00°	7.50°	0.00°	−7.50°	−15.00°	−22.50°	−30.00°	−37.50°	−45.00°

TABLE II. The setting angles of the HWPs (or QWP) for the projective measurement stage. Here "−" denotes the corresponding WP is removed from the optical circuit.

Observable	H2	H3	H4	Q4	H5	Q5	H6	H7
J_x	45.00°	−17.63°	75.00°	–	45.00°	–	0.00°	−62.63°
J_x^2	45.00°	90.00°	0.00°	–	45.00°	–	0.00°	22.50°
J_y	45.00°	17.63°	−15.00°	–	45.00°	–	0.00°	−62.63°
J_y^2	45.00°	90.00°	90.00°	–	45.00°	–	0.00°	22.50°
J_z	45.00°	0.00°	45.00°	–	45.00°	–	0.00°	−45.00°
$C_\pm(\lvert\psi_\phi^\perp\rangle_{\rm opt})$	45.00°	0.00°	45.00°	–	45.00°	–	0.00°	−45.00°
$C_\pm(\lvert\psi_{\pi/12}^\perp\rangle_1)$	45.00°	0.00°	45.00°	–	45.00°	–	−32.93°	−45.00°
$C_\pm(\lvert\psi_{\pi/12}^\perp\rangle_2)$	45.00°	0.00°	45.00°	–	45.00°	–	−37.74°	−45.00°
$C_\pm(\lvert\psi_{\pi/12}^\perp\rangle_3)$	45.00°	0.00°	45.00°	–	45.00°	–	−40.75°	−45.00°
$C_\pm(\lvert\psi_{\pi/6}^\perp\rangle_1)$	45.00°	0.00°	45.00°	–	45.00°	–	−24.55°	−45.00°
$C_\pm(\lvert\psi_{\pi/6}^\perp\rangle_2)$	45.00°	0.00°	45.00°	–	45.00°	–	−31.72°	−45.00°
$C_\pm(\lvert\psi_{\pi/6}^\perp\rangle_3)$	45.00°	0.00°	45.00°	–	45.00°	–	−36.95°	−45.00°
$C_\pm(\lvert\psi_{\pi/4}^\perp\rangle_1)$	45.00°	0.00°	45.00°	–	45.00°	–	−19.62°	−45.00°
$C_\pm(\lvert\psi_{\pi/4}^\perp\rangle_2)$	45.00°	0.00°	45.00°	–	45.00°	–	−27.37°	−45.00°
$C_\pm(\lvert\psi_{\pi/4}^\perp\rangle_3)$	45.00°	0.00°	45.00°	–	45.00°	–	−33.90°	−45.00°
$C_\pm(\lvert\psi_{\pi/3}^\perp\rangle_1)$	45.00°	0.00°	45.00°	–	45.00°	–	0.00°	−69.55°
$C_\pm(\lvert\psi_{\pi/3}^\perp\rangle_2)$	45.00°	0.00°	45.00°	–	45.00°	–	0.00°	−76.72°
$C_\pm(\lvert\psi_{\pi/3}^\perp\rangle_3)$	45.00°	0.00°	45.00°	–	45.00°	–	0.00°	−81.95°
$C_\pm(\lvert\psi_{5\pi/12}^\perp\rangle_1)$	45.00°	0.00°	45.00°	–	45.00°	–	0.00°	−77.92°
$C_\pm(\lvert\psi_{5\pi/12}^\perp\rangle_2)$	45.00°	0.00°	45.00°	–	45.00°	–	0.00°	−82.74°
$C_\pm(\lvert\psi_{5\pi/12}^\perp\rangle_3)$	45.00°	0.00°	45.00°	–	45.00°	–	0.00°	−85.75°
$C_\pm(\lvert\psi_{\pi/2}^\perp\rangle_1)$	45.00°	0.00°	45.00°	–	45.00°	–	0.00°	−45.00°
$C_\pm(\lvert\psi_{\pi/2}^\perp\rangle_2)$	45.00°	0.00°	45.00°	–	45.00°	–	0.00°	−45.00°
$C_\pm(\lvert\psi_{\pi/2}^\perp\rangle_3)$	45.00°	0.00°	45.00°	–	45.00°	–	0.00°	−45.00°
$C_\pm(\lvert\psi_{7\pi/12}^\perp\rangle_1)$	45.00°	0.00°	45.00°	–	45.00°	–	0.00°	−77.92°
$C_\pm(\lvert\psi_{7\pi/12}^\perp\rangle_2)$	45.00°	0.00°	45.00°	–	45.00°	–	0.00°	−82.74°
$C_\pm(\lvert\psi_{7\pi/12}^\perp\rangle_3)$	45.00°	0.00°	45.00°	–	45.00°	–	0.00°	−85.75°
$C_\pm(\lvert\psi_{2\pi/3}^\perp\rangle_1)$	45.00°	0.00°	45.00°	–	45.00°	–	0.00°	−69.55°
$C_\pm(\lvert\psi_{2\pi/3}^\perp\rangle_2)$	45.00°	0.00°	45.00°	–	45.00°	–	0.00°	−76.72°
$C_\pm(\lvert\psi_{2\pi/3}^\perp\rangle_3)$	45.00°	0.00°	45.00°	–	45.00°	–	0.00°	−81.95°
$C_\pm(\lvert\psi_{3\pi/4}^\perp\rangle_1)$	45.00°	0.00°	45.00°	–	45.00°	–	0.00°	−64.62°
$C_\pm(\lvert\psi_{3\pi/4}^\perp\rangle_2)$	45.00°	0.00°	45.00°	–	45.00°	–	0.00°	−72.37°
$C_\pm(\lvert\psi_{3\pi/4}^\perp\rangle_3)$	45.00°	0.00°	45.00°	–	45.00°	–	0.00°	−78.90°
$C_\pm(\lvert\psi_{5\pi/6}^\perp\rangle_1)$	45.00°	0.00°	45.00°	–	45.00°	–	−24.55°	−45.00°
$C_\pm(\lvert\psi_{5\pi/6}^\perp\rangle_2)$	45.00°	0.00°	45.00°	–	45.00°	–	−31.72°	−45.00°
$C_\pm(\lvert\psi_{5\pi/6}^\perp\rangle_3)$	45.00°	0.00°	45.00°	–	45.00°	–	36.95°	−45.00°
$C_\pm(\lvert\psi_{11\pi/12}^\perp\rangle_1)$	45.00°	0.00°	45.00°	–	45.00°	–	−32.93°	−45.00°
$C_\pm(\lvert\psi_{11\pi/12}^\perp\rangle_2)$	45.00°	0.00°	45.00°	–	45.00°	–	−37.74°	−45.00°
$C_\pm(\lvert\psi_{11\pi/12}^\perp\rangle_3)$	45.00°	0.00°	45.00°	–	45.00°	–	−40.75°	−45.00°
$C_\pm(\lvert\psi_\pi^\perp\rangle_1)$	45.00°	0.00°	45.00°	–	45.00°	–	−45.00°	−45.00°
$C_\pm(\lvert\psi_\pi^\perp\rangle_2)$	45.00°	0.00°	45.00°	–	45.00°	–	−45.00°	−45.00°
$C_\pm(\lvert\psi_\pi^\perp\rangle_3)$	45.00°	0.00°	45.00°	–	45.00°	–	−45.00°	−45.00°
$D(\lvert\psi_\phi^\perp\rangle_{J_x+J_y})$	45.00°	45.00°	–	45.00°	–	45.00°	0.00°	−90.00°

transformations of these optical elements. The measurement of observable J_x can be realized via six HWPs and three BDs. The unitary operation which performs the measurement on the qutrit can be written as

$$U = \begin{pmatrix} \frac{1}{2} & -\frac{1}{\sqrt{2}} & \frac{1}{2} \\ -\frac{1}{\sqrt{2}} & 0 & \frac{1}{\sqrt{2}} \\ \frac{1}{2} & \frac{1}{\sqrt{2}} & \frac{1}{2} \end{pmatrix} = U_3 U_2 U_1, \qquad \text{(A1)}$$

where we have

$$U_1 = \begin{pmatrix} 1 & 0 & 0 \\ 0 & \sqrt{\frac{2}{3}} & -\frac{1}{\sqrt{3}} \\ 0 & -\frac{1}{\sqrt{3}} & -\sqrt{\frac{2}{3}} \end{pmatrix}, \quad U_2 = \begin{pmatrix} \frac{1}{2} & -\frac{\sqrt{3}}{2} & 0 \\ \frac{\sqrt{3}}{2} & \frac{1}{2} & 0 \\ 0 & 0 & 1 \end{pmatrix},$$

$$U_3 = \begin{pmatrix} 1 & 0 & 0 \\ 0 & -\sqrt{\frac{2}{3}} & -\frac{1}{\sqrt{3}} \\ 0 & \frac{1}{\sqrt{3}} & -\sqrt{\frac{2}{3}} \end{pmatrix}. \qquad \text{(A2)}$$

The three unitary operations U_i $(i = 1,2,3)$ can be implemented by a single-qubit rotation on two of the three modes, keeping the other one unchanged.

The HWP (H3) at -17.63° is applied on the lower mode and implements a rotation

$$\begin{pmatrix} \sqrt{\frac{2}{3}} & -\frac{1}{\sqrt{3}} \\ -\frac{1}{\sqrt{3}} & -\sqrt{\frac{2}{3}} \end{pmatrix}$$

on the polarizations of photons in this mode, while it keeps the polarizations of the photons in the upper mode unchanged. Thus U_1 is realized. The HWP (H2) at 45° changes the polarizations of the photons in the upper mode from horizontal to vertical and after BD_{ii} the vertically polarized photons go straight and are still in the upper mode, whereas the horizontally polarized photons in the lower mode go up into the upper mode. Then we can realize a rotation

$$\begin{pmatrix} -\frac{\sqrt{3}}{2} & \frac{1}{2} \\ \frac{1}{2} & \frac{\sqrt{3}}{2} \end{pmatrix}$$

on the polarizations of photons in the upper mode via H4 at 75° and keep the polarizations of photons in the lower mode unchanged. Thus U_2 is realized. Similarly, we use H5 and BD_{iii} to move the photons with different polarization into the lower mode and use H7 at -62.63° to realize a rotation

$$\begin{pmatrix} -\frac{1}{\sqrt{3}} & -\sqrt{\frac{2}{3}} \\ -\sqrt{\frac{2}{3}} & \frac{1}{\sqrt{3}} \end{pmatrix}$$

and keep the polarization of photons in the upper mode unchanged. The HWP (H6) at zero is used as an optical compensator. Thus U_3 is realized.

The basis states of the qutrit, $|0\rangle$, $|1\rangle$, and $|2\rangle$, are encoded by the horizontal polarization of the photon in the upper mode, $|H_u\rangle$, the horizontal polarization of the photon in the lower mode, $|H_d\rangle$, and the vertical polarization in the lower mode, $|V_d\rangle$, respectively. The initial state

$$|\phi\rangle = \sin\phi|H_u\rangle + \cos\phi|V_d\rangle \tag{A3}$$

becomes

$$\sin\phi|H_u\rangle - \frac{1}{\sqrt{3}}\cos\phi|H_d\rangle - \sqrt{\frac{2}{3}}\cos\phi|V_d\rangle \tag{A4}$$

after H3 is applied on the polarizations of photons in the lower mode. After H2 is applied, it becomes

$$\sin\phi|V_u\rangle - \frac{1}{\sqrt{3}}\cos\phi|H_d\rangle - \sqrt{\frac{2}{3}}\cos\phi|V_d\rangle. \tag{A5}$$

Going through the following BD (BD_{ii}), the state is

$$-\frac{1}{\sqrt{3}}\cos\phi|H_u\rangle + \sin\phi|V_u\rangle - \sqrt{\frac{2}{3}}\cos\phi|V_d\rangle. \tag{A6}$$

The HWP (H4) is applied on the polarizations of photons in the upper mode and the state becomes

$$\frac{1}{2}(\cos\phi + \sin\phi)|H_u\rangle + \left(-\frac{1}{2\sqrt{3}}\cos\phi + \frac{\sqrt{3}}{2}\sin\phi\right)|V_u\rangle - \sqrt{\frac{2}{3}}\cos\phi|V_d\rangle. \tag{A7}$$

After H5 is applied on the photons in the lower mode, $|V_d\rangle$ is rotated to $|H_d\rangle$. Going through the following BD_{iii}, the state is

$$\frac{1}{2}(\cos\phi + \sin\phi)|H_u\rangle - \sqrt{\frac{2}{3}}\cos\phi|H_d\rangle + \left(-\frac{1}{2\sqrt{3}}\cos\phi + \frac{\sqrt{3}}{2}\sin\phi\right)|V_d\rangle. \tag{A8}$$

The HWP (H7) is applied on the polarizations of photons in the lower mode and the state becomes

$$\frac{1}{2}(\cos\phi + \sin\phi)|H_u\rangle + \frac{1}{\sqrt{2}}(\cos\phi - \sin\phi)|H_d\rangle + \frac{1}{2}(\cos\phi + \sin\phi)|V_d\rangle, \tag{A9}$$

which is the same as $U|\phi\rangle$.

APPENDIX B: VERIFY THE NEW UNCERTAINTY RELATIONS WITH A TWO-LEVEL SYSTEM

We choose $A = \sigma_x$ and $B = \sigma_y$, and a family of states being measured $|\psi_\phi\rangle = \sin\phi|+\rangle + \cos\phi|-\rangle$, where $|\pm\rangle$ are the eigenstates of $\sigma_z = -i[\sigma_x,\sigma_y]/2$ corresponding to the eigenvalues ±1. Similar to the case of a qutrit, for the special states with $\phi = \pi/4$ and $\phi = 3\pi/4$, the Heisenberg-Robertson relation can be trivial because one of the variances of measurements is zero. The new uncertainty relations are valid for all the states, including those with $\phi = \pi/4$ and $\phi = 3\pi/4$.

There is only one state $|\psi_\phi^\perp\rangle = \cos\phi|0\rangle - \sin\phi|1\rangle$ which is orthogonal to the qubit state $|\psi_\phi\rangle$ and it is the optimal choice for the first inequality,

$$\Delta A^2 + \Delta B^2 \geqslant \pm i\langle[A,B]\rangle + |\langle\psi|A \pm iB|\psi^\perp\rangle|^2, \tag{B1}$$

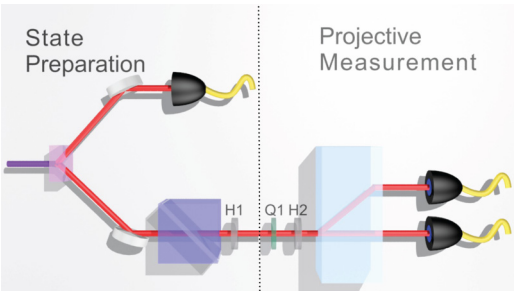

FIG. 3. Experimental setup. The herald single photons are created via type I SPDC in a BBO crystal and are injected into the optical network. The PBS and HWP (H1) are used to generate a qubit state $|\psi_\phi\rangle$. The HWP (or QWP) and the following BD are used to realize the projective measurements of observables $\sigma_{x(y)}$, $\sigma^2_{x(y)}$, $C_\pm$, and D.

TABLE III. The setting angles of Q1 and H2 for the projective measurement stage of the two-level system. Here "−" denotes that Q1 is removed from the optical circuit.

Observable	Q1	H2
σ_x	−	22.50°
σ_y	90.00°	22.50°
σ_x^2,σ_y^2	−	0.00°
σ_z	−	0.00°
$C_\pm(\lvert\psi_\phi^\perp\rangle)$	−	0.00°
$D(\lvert\psi_\phi^\perp\rangle_{\sigma_x+\sigma_y})$	90.00°	$\frac{(\phi-\frac{\pi}{2})}{2}$

which becomes an identical equation. This state is also the only choice for testing the uncertainty inequality in

$$\Delta A^2 + \Delta B^2 \geqslant \tfrac{1}{2}|_{A+B}\langle\psi^\perp|A+B|\psi\rangle|^2. \tag{B2}$$

The observables

$$C_\pm := (\sigma_x \pm i\sigma_y)|\psi_\phi^\perp\rangle\langle\psi_\phi^\perp|(\sigma_x \mp i\sigma_y) \tag{B3}$$

and

$$D := \tfrac{1}{2}(\sigma_x+\sigma_y)|\psi_\phi^\perp\rangle\langle\psi_\phi^\perp|(\sigma_x+\sigma_y) \tag{B4}$$

are the same as those for the qutrit case in the main text and for the qubit case, i.e., $J_{x,y,z} = \sigma_{x,y,z}$ and $|\psi_\phi^\perp\rangle_{\sigma_x+\sigma_y} = |\psi_\phi^\perp\rangle$.

For experimental demonstration shown in Fig. 3, we prepare a qubit state with the basis states $|0\rangle$ and $|1\rangle$ encoded in the horizontal and vertical polarizations of heralded single photons via type I SPDC. By changing the setting angle of the HWP (H1) which applies a rotation on the polarization qubit, we can obtain the qubit state $|\psi_\phi\rangle$ for 12 values of ϕ. For measurement, a BD and a HWP (or a QWP) are used to implement measurements of observables σ_x, σ_y, σ_z, σ_x^2, σ_y^2, $C_\pm^\perp$, and D. The setting angles of the HWP and QWP are shown in Table III.

In Fig. 4, we show the direct demonstrations of the new uncertainty relations in inequalities (B1) and (B2). The solid black line corresponds to theoretical predictions of the left-hand sides of inequalities (B1) and (B2), i.e., $\Delta\sigma_x^2 + \Delta\sigma_y^2$. The black squares represent the sum of the measured uncertainties ($\Delta\sigma_x^2$ and $\Delta\sigma_y^2$) with the 12 states. The green circles represent the experimental results of the right-hand side of inequality (B1) with the state $|\psi^\perp\rangle$. The red dotted line corresponds to the bound of inequality (B2) and the red stars represent the measured $\langle D\rangle$ for the 12 states $|\psi^\perp\rangle$. The blue dot-dashed curves and triangles represent the theoretical predictions and experimental results of the product of the uncertainties and the expectation value of the commutator (the Heisenberg-Robertson relation).

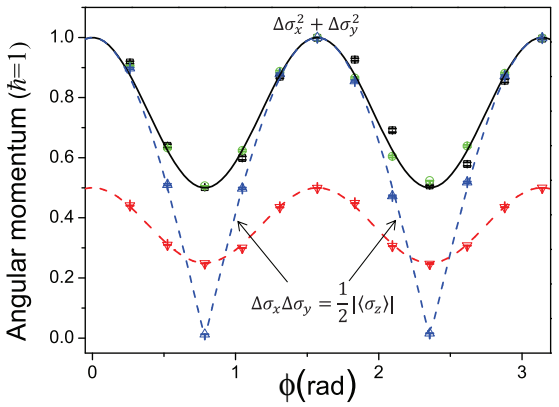

FIG. 4. Experimental results. The solid black line corresponds to the LHS of inequalities (B1) and (B2). The black squares represent the sum of the measured uncertainties of $\Delta\sigma_x^2$ and $\Delta\sigma_y^2$ with the 12 states $|\psi_\phi\rangle$. The green circles represent the experimental results of the RHS of inequality (B1) with the optimal and only state $|\psi_\phi^\perp\rangle$ for each of the 12 values of ϕ. The red dotted line corresponds to the bound of inequality (B2) and red stars represent the measured $\langle D\rangle$ for the 12 states $|\psi_\phi^\perp\rangle$. The blue dot-dashed curves and triangles represent the theoretical predictions and experimental results of the product of the uncertainties and the expectation value of the commutator (Heisenberg-Robertson relation). Error bars indicate the statistical uncertainty.

All data from the right-hand side of inequality (B1) are above the lower curves, which are the product of the uncertainties and the expectation value of the commutator. Thus the new uncertainty relation in inequality (B1) is more strengthened compared to the Heisenberg-Robertson relation. Even for the special states with $\phi = \pi/4$ and $\phi = 3\pi/4$ which trivialize the Heisenberg-Robertson relation, the lower bounds of the new uncertainty inequalities (B1) and (B2) are always nontrivial.

As we said in the main text, although the new uncertainty relations are valid for two-level states, there is only one state which is orthogonal to the qubit state and it is the optimal choice for the first inequality, which becomes an identical equation. The qutrit case displays more features of the new uncertainty relations.

[1] W. Heisenberg, Z. Phys. **43**, 172 (1927).
[2] J. A. Wheeler and H. Zurek, *Quantum Theory and Measurement* (Princeton University Press, Princeton, NJ, 1983).
[3] H. P. Robertson, Phys. Rev. **34**, 163 (1929).
[4] M. J. W. Hall, Gen. Relativ. Gravit. **37**, 1505 (2005).
[5] P. Busch, T. Heinonen, and P. J. Lahti, Phys. Rep. **452**, 155 (2007).
[6] M. Ozawa, Phys. Rev. A **67**, 042105 (2003).
[7] M. Ozawa, Phys. Lett. A **320**, 367 (2004).
[8] M. Berta, M. Christandl, R. Colbeck, J. M. Renes, and R. Renner, Nat. Phys. **6**, 659 (2010).
[9] P. Busch, P. Lahti, and R. F. Werner, Rev. Mod. Phys. **86**, 1261 (2014).
[10] W. P. Bowen, R. Schnabel, P. K. Lam, and T. C. Ralph, Phys. Rev. Lett. **90**, 043601 (2003).
[11] O. Gühne, Phys. Rev. Lett. **92**, 117903 (2004).
[12] J. C. Howell, R. S. Bennink, S. J. Bentley, and R. W. Boyd, Phys. Rev. Lett. **92**, 210403 (2004).

[13] C. A. Fuchs and A. Peres, Phys. Rev. A **53**, 2038 (1996).
[14] J. M. Renes and J. C. Boileau, Phys. Rev. Lett. **103**, 020402 (2009).
[15] J. Erhart, S. Sponar, G. Sulyok, G. Badurek, M. Ozawa, and Y. Hasegawa, Nat. Phys. **8**, 185 (2012).
[16] G. Sulyok, S. Sponar, J. Erhart, G. Badurek, M. Ozawa, and Y. Hasegawa, Phys. Rev. A **88**, 022110 (2013).
[17] G. Sulyok, S. Sponar, Bülent Demirel, F. Buscemi, M. J. W. Hall, M. Ozawa, and Y. Hasegawa, Phys. Rev. Lett. **115**, 030401 (2015).
[18] C.-F. Li, J.-S. Xu, X.-Y. Xu, K. Li, and G.-C. Guo, Nat. Phys. **7**, 752 (2011).
[19] R. Prevedel, D. R. Hamel, R. Colbeck, K. Fisher, and K. J. Resch, Nat. Phys. **7**, 757 (2011).
[20] L. A. Rozema, A. Darabi, D. H. Mahler, A. Hayat, Y. Soudagar, and A. M. Steinberg, Phys. Rev. Lett. **109**, 100404 (2012).
[21] M. M. Weston, M. J. W. Hall, M. S. Palsson, H. M. Wiseman, and G. J. Pryde, Phys. Rev. Lett. **110**, 220402 (2013).
[22] M. Ringbauer, D. N. Biggerstaff, M. A. Broome, A. Fedrizzi, C. Branciard, and A. G. White, Phys. Rev. Lett. **112**, 020401 (2014).
[23] F. Kaneda, S.-Y. Baek, M. Ozawa, and K. Edamatsu, Phys. Rev. Lett. **112**, 020402 (2014).
[24] L. Maccone and A. K. Pati, Phys. Rev. Lett. **113**, 260401 (2014).
[25] Although the new uncertainty relations are valid for two-level states (see more details in the Appendix), there is only one state which is orthogonal to the qubit state and it is the optimal choice for the first inequality, which becomes an identical equation. The qutrit case displays more features of the new uncertainty relations.
[26] W. Elion, M. Matters, U. Geigenmuller, and J. Mooij, Nature (London) **371**, 594 (1994).
[27] O. Nairz, M. Arndt, and A. Zeilinger, Phys. Rev. A **65**, 032109 (2002).
[28] M. D. LaHaye, O. Buu, B. Camarota, and K. C. Schwab, Science **304**, 74 (2004).
[29] A. Schliesser, O. Arcizet, R. Riviere, G. Anetsberger, and T. J. Kippenberg, Nat. Phys. **5**, 509 (2009).
[30] B. Jack, P. Aursand, S. Franke-Arnold, D. G. Ireland, J. Leach, S. M. Barnett, and M. J. Padgett, J. Opt. **13**, 064017 (2011).
[31] P. Xue, R. Zhang, H. Qin, X. Zhan, Z. H. Bian, J. Li, and B. C. Sanders, Phys. Rev. Lett. **114**, 140502 (2015).
[32] Z. H. Bian, J. Li, H. Qin, X. Zhan, R. Zhang, B. C. Sanders, and P. Xue, Phys. Rev. Lett. **114**, 203602 (2015).
[33] P. Xue, R. Zhang, Z. H. Bian, X. Zhan, H. Qin, and B. C. Sanders, Phys. Rev. A **92**, 042316 (2015).
[34] P. Xue, H. Qin, B. Tang, and B. C. Sanders, New J. Phys. **16**, 053009 (2014).
[35] X. Zhan, X. Zhang, J. Li, Y. S. Zhang, B. C. Sanders, and P. Xue, Phys. Rev. Lett. **116**, 090401 (2016).
[36] X. Zhan, J. Li, H. Qin, Z. H. Bian, and P. Xue, Opt. Exp. **23**, 18422 (2015).
[37] J. Ahrens, E. Amselem, A. Cabello, and M. Bourennane, Sci. Rep. **3**, 2170 (2013).
[38] D. J. Rowe, B. C. Sanders, and H. de Guise, J. Math. Phys. **40**, 3604 (1999).
[39] H. P. Yuen, Phys. Rev. Lett. **51**, 719 (1983).
[40] M. Ozawa, Phys. Rev. Lett. **60**, 385 (1988).
[41] J. Maddox, Nature (London) **331**, 222 (1988).